Great Pending Himalaya Earthquakes

Steven G. Wesnousky*[1]

Abstract

Geological, historical, and geophysical observations show that the entire Himalayan arc is poised to produce a sequence of great earthquakes, possibly similar to that which occurred in the twentieth century along the Aleutian subduction zone. The human catastrophe in the densely populated countries astride the arc is likely to be unprecedented when these earthquakes occur.

Cite this article as Wesnousky, S. G. (2020). Great Pending Himalaya Earthquakes, *Seismol. Res. Lett.* **XX**, 1–9, doi: 10.1785/0220200200.

Supplemental Material

Introduction

Historical reports of earthquake damage provide the earliest evidence of great earthquakes along the Himalayan arc (Iyengar *et al.*, 1999; Pant, 2002). The tectonic framework explaining the genesis of these earthquakes came with the advent of plate tectonics (Isacks *et al.*, 1968), the recognition of the tectonic similarity of the Himalayan arc with oceanic-subduction zones (Molnar *et al.*, 1977; Seeber and Armbruster, 1981; Molnar and Lyon-Caen, 1983), and ensuing advances in geodesy (Bilham *et al.*, 1997). Today it is generally accepted that the largest earthquakes along the Himalayan arc are the episodic release of stress that accumulates with the convergence of India into Tibet (Fig. 1, bottom left inset). The largest earthquake displacements along the arc occur on a shallow-dipping décollement that reaches ≥100 km in width: the Main Himalayan thrust (MHT; Fig. 1, top right inset). The southernmost intersection of the décollement with the surface forms the trace of the Himalayan Frontal thrust (HFT). The Main Boundary thrust is an older splay off the MHT that intersects the surface north of the HFT. The largest earthquakes that rupture the décollement extend to the surface to deform and fault young sediments along the HFT (Nakata, 1972, 1989). Where preserved, these deformations provide a record of the timing and amount of displacement that has occurred during the largest geologically recent great earthquakes along the arc and the average rate at which slip accrues on the MHT. Here, I synthesize paleoearthquake data along the Himalayan arc in the context of geophysical observation and history in consideration of the size and timing of great earthquakes that may be expected in the future. The synthesis complements prior studies that have brought awareness to the hazard and risk posed by Himalayan earthquakes (e.g., Bilham *et al.*, 2001; Rajendran *et al.*, 2015, 2017; Wyss *et al.*, 2018; Bilham, 2019).

Observations and Evaluation

Geologic estimates of the rate at which slip accrues and the timing and size of past earthquake displacements are now reported at nearly 30 sites along ~2000 km of the Himalayan arc (Table 1 and Fig. 1a). Geologically recent displacements are generally recorded by the presence of fluvial terraces that are uplifted and abandoned by displacement on the underlying HFT (Nakata, 1972; Wesnousky *et al.*, 1999) (Fig. 2a). The vertical component of the rate of displacement (uplift) is acquired by measuring the height of a terrace above modern stream grade and collecting detrital charcoal samples from sediments capping the abandoned terraces. Dividing the height of the terrace by the age of the radiocarbon samples yields an estimate of the average uplift rate. Uplift rates estimated in this way may be minimum values of that rate: samples of detrital charcoal used to date uplifted hanging wall terrace capping sediments can be older than the sediment in which they are hosted (Blong and Gillespie, 1978), and correlative footwall terrace surfaces are tectonically buried at unknown depths beneath the modern river grade. Estimates that have been reported are summarized in Table 1 and shown as red bars in Figure 1b. Geodesy provides a measure of the convergence rate that is accommodated by southward propagation of slip on the décollement, which may be compared to geologic estimates of the uplift rate with knowledge of the HFT fault dip. The few direct measures of fault dip arising from borehole, seismic reflection, and structural analyses place the dip of the HFT in the range of 30° ± 10° (Rao *et al.*, 1974; Lyon-Caen and Molnar, 1985; Raiverman *et al.*, 1993; Powers *et al.*, 1998; Bollinger *et al.*, 2014; Almeida *et al.*, 2018). Geodetic analyses (Vernant *et al.*, 2014; Zheng *et al.*, 2017; Lindsey *et al.*, 2018; Bilham, 2019; Ingleby *et al.*, 2020) indicate that $\sim 15 \pm 2$ mm/yr of the convergence between India and Eurasia is accumulating as strain that may be released by slip during large earthquakes on the MHT (green bar in Fig. 1b). The 15 ± 2 mm/yr shortening rate equates to a 7.5 ± 1 mm/yr vertical uplift rate when slip is on a 30° dipping fault (orange bar in Fig. 1b). The value falls within the range of estimates arising from geology.

1. Center for Neotectonic Studies and Nevada Seismological Laboratory, University of Nevada, Reno, Nevada, U.S.A.

*Corresponding author: wesnousky@unr.edu

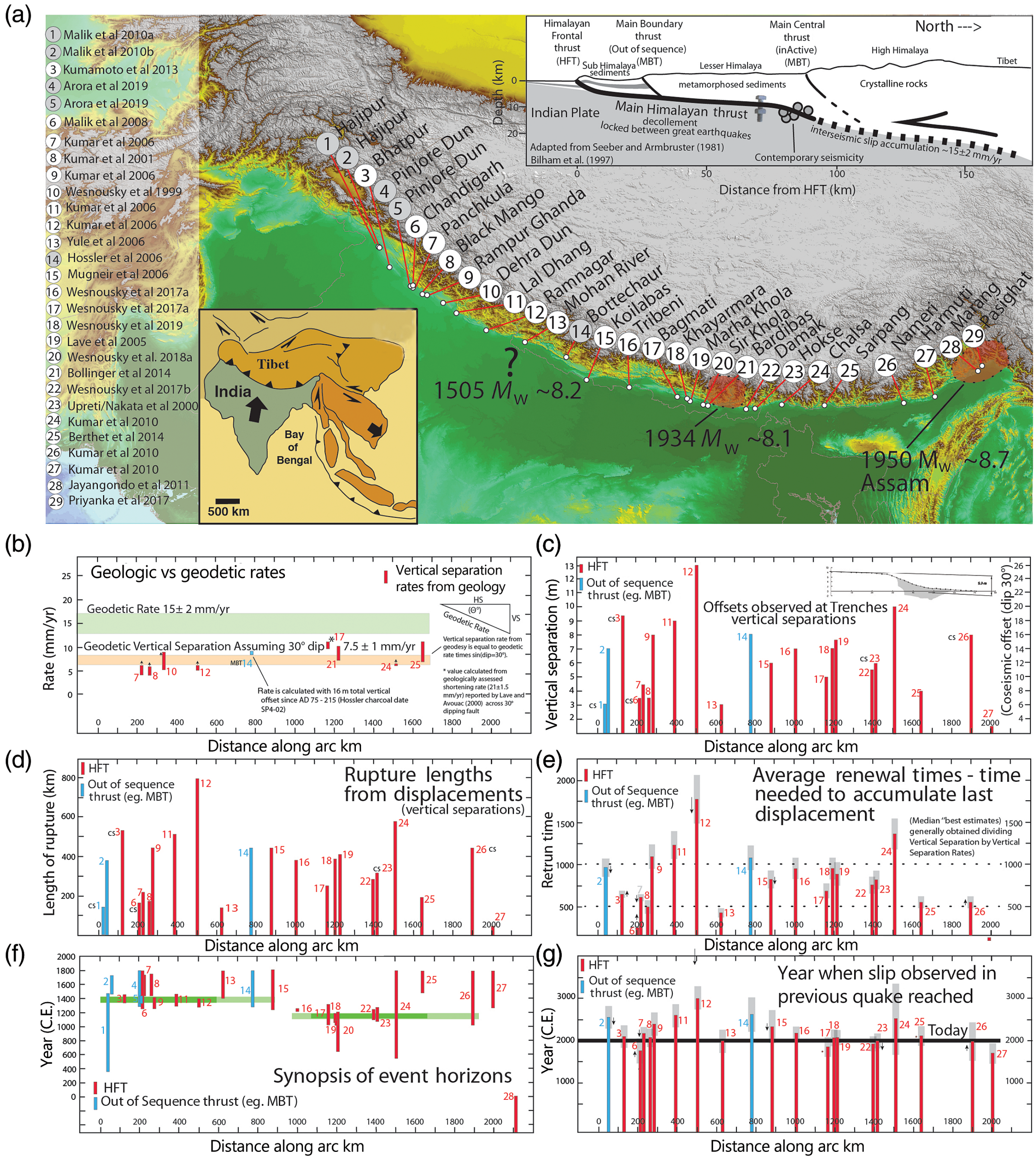

Figure 1. (a) Locations and citations of paleoearthquake and fault-slip rate studies along Himalayan Frontal thrust (HFT) (white circles), and out of sequence thrusts (gray circles). One out of sequence site (14) is on the Main Boundary thrust (MBT) and the remainder on fault traces within ~3–5 km of the HFT. Numbers correspond to Table 1. (Bottom left inset) Plate tectonic framework, (top right inset) generalized north–south cross-section transverse to Himalayan arc shows location of Main Himalayan thrust (MHT) décollement and intersections with surface that define the HFT and MBT and location of contemporary moderate size earthquakes. Dates of largest known earthquakes and reported areas of greatest shaking are annotated. (b–g) Data of Table 1 plotted as function of distance along arc. The color version of this figure is available only in the electronic edition.

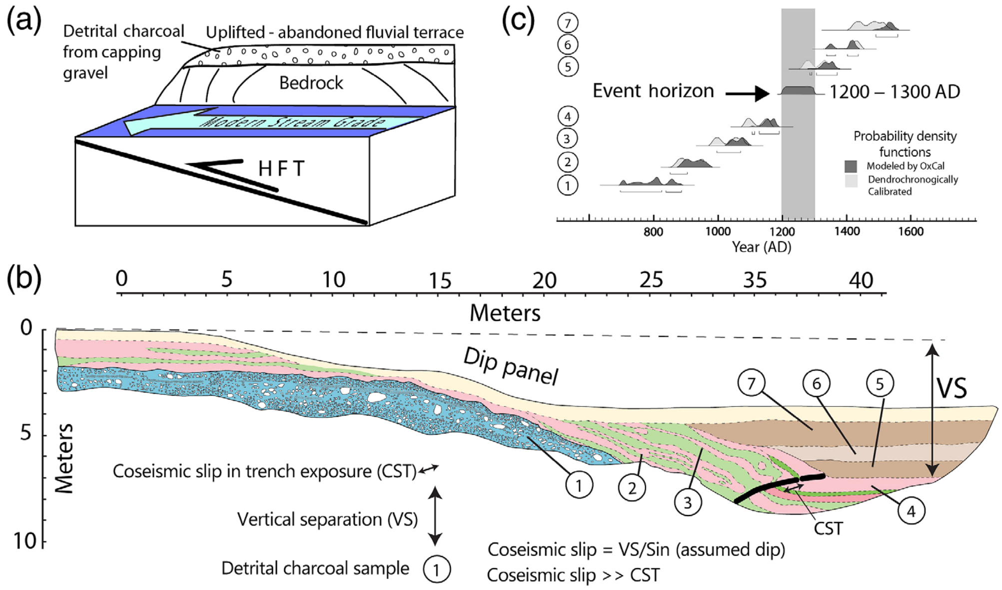

Figure 2. Concepts, methods, and observations used in assessing uplift rate, timing, and size of past earthquakes from geology. (a) Detrital charcoal in capping deposit of uplifted, incised, and abandoned terrace as result of displacement on underlying HFT. (b) Trench exposure illustrating characteristics of deformation commonly observed near surface resulting from fault displacement on the HFT. Location of 7 hypothetical charcoal samples are numbered. (c) Ages of the 7 charcoal samples are expressed as probabilty density functions and arranged according to age and stratigraphic level. The color version of this figure is available only in the electronic edition.

Structural, stratigraphic, soil, and radiocarbon analysis of sediments broken and deformed by displacement on the HFT form the crux of geological observation bearing on the size and timing of past earthquakes. Exposures of deformed sediments are generally obtained by excavation of trenches across scarps produced during the most recent movements on the HFT. The sketch in Figure 2b illustrates the types of deformation and deposits typically observed in trench exposures emplaced across scarps of the HFT and the manner in which the timing and amount of displacement in past earthquakes is determined. Deposits exposed are most frequently fluvial rounded cobble gravel (blue) overlain by fine sand and silt (pink and green) flood deposits. Fault displacement toward the surface is increasingly accommodated by folding, such that fault scarps are largely the result of folding and not simple fault displacement (Wesnousky *et al.*, 2019). The folding is manifest by a dip panel, and displacement of any piercing points across observed fault strands are at best a minimum of the actual fault displacement required to produce the attendant scarp (e.g., coseismic slip in trench exposure in Fig. 2b). Estimates of vertical separation (VS) may accurately be measured across the scarp and provide a minimum measure of the actual fault displacement responsible for forming the scarp. The values reported at each site are displayed in Figure 1c and Table 1 and commonly range between 5 and 10 m. Confident measure of the actual displacement on the underlying thrust required to produce the observed VS is generally compromised because the dip of the thrust plane immediately beneath the scarp is too deep to be observed. It is commonly assumed that the dip is 30°, in which case the coseismic slip required to produce a scarp will be twice the observed VS.

Drawing upon scaling relationships that compare the average displacement during modern plate boundary thrust earthquakes to their respective rupture lengths (Leonard, 2010), the observed VSs in Figure 1c are considered proxies for coseismic offset and are converted to rupture lengths in Figure 1d. The predicted lengths are commonly between 300 and 500 km commensurate with earthquakes with $M_w > \sim 8.5$ (Table 1 and Table S1, available in the supplemental material to this article), values that are considered minima because actual fault displacements are likely larger than the observed VSs. The length of predicted ruptures is commonly greater than the distance between sites, and rupture of many adjacent sites may reasonably be assumed to have occurred simultaneously. These observations alone are insufficient to conclude which sites did indeed rupture simultaneously; though they make clear that earthquakes of $M_w > 8.5$ and rupture lengths of 300–500 km or greater have occurred along the arc.

The calculated time that it will take for interseismic convergence to equal the observed coseismic displacement at a trench (renewal interval) is commonly used to approximate the average expected time interval (repeat time) between fault displacements. Estimates of average renewal intervals at each site are shown in Figure 1e and are determined by dividing the observed VSs in Figure 1c by the 7.5 ± 1 mm/yr VS rate illustrated in Figure 1b. Most of the values fall between 500 and 1000 yr (horizontal dotted lines). The scatter in estimated repeat times occurs in part because coseismic surface rupture displacements in Himalayan earthquakes likely show significant variability along strike (Wesnousky, 2008), and the repeat times are estimated with a common interseismic slip accumulation rate. Uncertainty bars (gray) in Figure 1e for the individual values reflect the ±1 mm/yr uncertainty attached to the VS rate and generally are on the order of 100s of years. Considering a range of dips around the assumed 30° dip used

TABLE 1
Data Summary

Number	Location*	Distance (km)†	Event Horizon Lower Bound‡	Event Horizon Upper Bound	Offset (m)§	Rupture Length (km)‖	M_w#	Geologic Vertical Rate (mm/yr)**	Renewal Time (yr)††	Next C.E.‡‡	Reference	Notes§§
1	[Hajipur HF2]	42	380	1479	[≥ 3]	136	7.8		≥204 ± 14		Malik, Sahoo, *et al.* (2010)	a
2	[Hajipur HF2]	44	1479	1749	≤7	377	8.6		≤950 ± 127	≤2564 ± 262	Malik, Shah, *et al.* (2010)	b
3	Bhatpur	126	1340	1461	[≥ 9.3]	530	8.8		≥631 ± 84	≥2032 ± 145	Kumahara and Jayangandoperumal (2013)	c
4	[Pinjore-PGF]	214	1288	1600							Arora *et al.* (2019)	d
5	[Pinjore-Jhajra]	215	1336	1441							Arora *et al.* (2019)	e
6	Chandigarh	219	1255	1800	[≥ 3.5]	164	8.0		≥238 ± 32	≥1765 ± 304	Malik *et al.* (2008)	f
7	Panchkula	222	1441	1600	≤4.4	216	8.2	5.0 ± 1	≤597 ± 80	≤2118 ± 159	Kumar *et al.* (2006)	g
8	Black Mango	262	1445	1756	3.6	170	8.0	4.8 ± 0.9	489 ± 65	2089 ± 221	Kumar *et al.* (2001)	h
9	Rampur Ghanda	278	1260	1421	8	443	8.7		1086 ± 145	2426 ± 225	Kumar *et al.* (2006)	i
10	Dehra Dun	333						6.9 ± 1.8			Wesnousky *et al.* (1999)	ij
11	Lal Dhang	390	1296	1470	9	510	8.8		1222 ± 163	2605 ± 250	Kumar *et al.* (2006)	j
12	Ramnagar	504	1281	1405	<13	793	9.1	5.5 ± 0.5	<1765 ± 235	<3108 ± 297	Kumar *et al.* (2006)	k
13	Mohan River	627	1410	1800	3	136	7.8		407 ± 54	2012 ± 249	Yule *et al.* (2006)	l
14	[Bottechaur]	778	1284	1800	8	443	8.7	8.6 ± 0.4	1086 ± 145	2628 ± 403	Hossler *et al.* (2016)	m
15	Koilabas	880	1240	1815	≤6	313	8.4		≤814 ± 109	≤2342 ± 396	Mugnier *et al.* (2005)	n
16	Tribeni	1005	1221	1262	7	377	8.6		950 ± 127	2192 ± 147	Wesnousky *et al.* (2017a)	o

*Site 14 (Bottechaur) on MBT. Sites 1 and 2 (Hajipur) and 4 and 5 (Pinjore Garden) are on out of sequence thrusts within ~3–5 km of the Himalayan Frontal thrust (HFT). All other sites are on HFT.

†Approximate distance along HFT from Pakistan border.

‡Event horizons recalculated with radiocarbon data provided in original studies. See the supplemental material.

§Geologic measure of displacement during last surface rupture: vertical separation (VS) except for values in brackets which are coseismic slip (CS). Values of VS are always a minimum value of the coseismic slip required to have produced the single-event fault scarps considered. The measures of VS and CS are considered the maximum or minimum bound when preceded by < and > symbols, respectively.

‖Rupture lengths computed from values of offset (VS or CS) using scaling relationship between displacement and rupture length for dip-slip earthquakes published in table 5 of Leonard (2010).

#Moment-magnitude M_w computed from rupture length using scaling relationship reported in table 6 of Leonard (2010).

**Geologic determinations of slip rate at sites along the HFT. All values are VS rates measured directly from uplifted and abandoned fluvial terraces dated with radiocarbon. Values are minimums with respect to observation that dating of terraces generally is accomplished with detrital charcoal beneath terrace surfaces. Detrital charcoal places a maximum bound on the age of sediment where it is deposited.

††Renewal time (repeat time) computed by dividing value in offset column by VS rate when value in offset column is VS. When value in offset column is CS, renewal time is estimated by dividing CS by the fault-slip rate. Calculations assume fault-slip rate equals geodetic rate of 15 ± 2 mm/yr and VS rate is $(15 \pm 2) \times \cos(30°)$.

‡‡Calculated year C.E. when accumulated displacement (strain) will equal that which occurred in last earthquake. Calculated by adding value in "Renewal Time" column to the bounding "Event Horizon" ages.

§§see Table S1.

(Continued next page.)

TABLE 1 (continued)
Data Summary

Number	Location*	Distance (km)†	Event Horizon Lower Bound‡	Event Horizon Upper Bound	Offset (m)§	Rupture Length (km)‖	M_w#	Geologic Vertical Rate (mm/yr)**	Renewal Time (yr)††	Next C.E.‡‡	Reference	Notes§§
17	Bagmati	1162	1031	1321	5	252	8.3	12.3 ± 0.8	679 ± 90	1855 ± 235	Wesnousky *et al.* (2017a)	p
18	Khayarmara	1200	1059	1195	7	377	8.6		950 ± 127	2077 ± 195	Wesnousky *et al.* (2019)	q
19	Marha Khola	1204	1022	1102	7.5	410	8.6		1018 ± 136	2080 ± 176	Lave *et al.* (2005)	r
20	Sir Khola	1210	644	1210							Wesnousky *et al.* (2018)	s
21	Bardibas	1217						8.5 ± 1.5			Bollinger *et al.* (2014)	st
22	Damak	1393	1100	1250	5.5	282	8.4		747 ± 100	1922 ± 175	Wesnousky *et al.* (2017b)	t
23	Hokse	1413	1078	1282	[~6]	313	8.4		814 ± 109	1994 ± 211	Upreti *et al.* (2000)	u
24	Chalsa	1507	544	1800	10	579	8.9	6.2 ± 0.1	1357 ± 181	2529 ± 809	Kumar *et al.* (2010)	v
25	Sarpang	1640	1485	1800	4	193	8.1	8.8 ± 2.1	543 ± 72	2185 ± 230	Berthet *et al.* (2014)	w
26	Nameri	1897	1025	1800	[≥ 8]	443	8.7			≥1955 ± 460	Kumar *et al.* (2010)	x
27	Harmutti	2000	1271	1800	1.2	45	7.0		163 ± 22	1698 ± 286	Kumar *et al.* (2010)	y
28	Marbang	2163	BC	BC							Jayangandoperumal *et al.* (2011)	z
29	Pasighat	2180									Priyanka *et al.* (2017)	zz

*Site 14 (Bottechaur) on MBT. Sites 1 and 2 (Hajipur) and 4 and 5 (Pinjore Garden) are on out of sequence thrusts within ~3–5 km of the Himalayan Frontal thrust (HFT). All other sites are on HFT.
†Approximate distance along HFT from Pakistan border.
‡Event horizons recalculated with radiocarbon data provided in original studies. See the supplemental material.
§Geologic measure of displacement during last surface rupture: vertical separation (VS) except for values in brackets which are coseismic slip (CS). Values of VS are always a minimum value of the coseismic slip required to have produced the single-event fault scarps considered. The measures of VS and CS are considered the maximum or minimum bound when preceded by < and > symbols, respectively.
‖Rupture lengths computed from values of offset (VS or CS) using scaling relationship between displacement and rupture length for dip-slip earthquakes published in table 5 of Leonard (2010).
#Moment-magnitude M_w computed from rupture length using scaling relationship reported in table 6 of Leonard (2010).
**Geologic determinations of slip rate at sites along the HFT. All values are VS rates measured directly from uplifted and abandoned fluvial terraces dated with radiocarbon. Values are minimums with respect to observation that dating of terraces generally is accomplished with detrital charcoal beneath terrace surfaces. Detrital charcoal places a maximum bound on the age of sediment where it is deposited.
††Renewal time (repeat time) computed by dividing value in offset column by VS rate when value in offset column is VS. When value in offset column is CS, renewal time is estimated by dividing CS by the fault-slip rate. Calculations assume fault-slip rate equals geodetic rate of 15 ± 2 mm/yr and VS rate is $(15 \pm 2) \times \cos(30°)$.
‡‡Calculated year C.E. when accumulated displacement (strain) will equal that which occurred in last earthquake. Calculated by adding value in "Renewal Time" column to the bounding "Event Horizon" ages.
§§see Table S1.

to calculate the VS rate would increase these uncertainty values. Notwithstanding the scatter and uncertainty, the observations suggest that sufficient slip accumulates in ~500–1000 yr to produce surface displacements like those documented at sites along the HFT.

The timing of earthquake displacements interpreted in trench exposures arises from arranging the age of detrital charcoal samples in the approximate stratigraphic order of the sedimentary unit from which they are sampled and separating them according to whether or not they are in faulted deposits. The simplified sketch of Figure 2b illustrates that detrital charcoal samples 1, 2, 3, and 4 are in sediments deformed and faulted, whereas samples 5, 6, and 7 are from sediments deposited after the last earthquake displacement (Fig. 2b,c). Radiocarbon ages are typically dendrochronologically corrected (Reimer *et al.*, 2013) and presented as probability distributions, which for example are colored light gray in Figure 2c. The bracket of time between the youngest sample from broken deposits and the oldest from unbroken deposits is the event horizon: the range of ages bracketing when the displacement producing the deformation occurred. It is common that sequences of dendrochronologically corrected ages are subject to OxCal (Ramsey, 1995, 2009), a program that uses Bayesian principles to estimate the most likely age of each sample such that stratigraphic order is satisfied and provides the user with a formal estimate of the event horizon. The darker probability distribution symbols in Figure 2c represent those subject to analysis by OxCal and, in this hypothetical example place, the event horizon between A.D. 1200 and 1300. Although the estimates made in this fashion are formalized, they do not generally incorporate errors posed by the residence time of charcoal in transport or contamination of sample collections by modern roots (Blong and Gillespie, 1978).

The approach nevertheless provides a consistent comparison of the timing of event horizons at adjacent sites along a fault zone and is used here with radiocarbon ages reported by investigators at each respective trench site along the arc. Plots like that shown in Figure 2c are archived for each site in Figure S1 and the calculated event horizons plotted in Figure 1f. The latter plot shows that the overlapping of event horizon ages along sections of the arc is consistent with the occurrence of ruptures reaching ~500 km in length (dark green bars). Allowing that event horizon age brackets may be slightly larger than formally calculated, the simultaneous rupture of ~800 km sections of the arc appears possible (light green bars). These rupture lengths are in concert with those predicted from observed offsets at the trench sites (Fig. 1d). Regardless of the exact rupture lengths and timing, when taken together, one may surmise that large earthquakes released a significant amount of accumulated strain along the central and western portion of the arc about A.D. 1200–1400, an observation previously put forth in the study of Kumar *et al.* (2010) and more recently discussed by Rajendran *et al.* (2015) and Bilham (2019).

Adding the estimates of the average renewal time (Fig. 1e) to the respective ages of the event horizon (Fig. 1f) at the respective sites yields an approximation of the expected next year of displacement (Fig. 1g). The calculated years of next displacement at each site are generally very near today. The simplest interpretation of the result is that virtually the entire arc has accumulated sufficient strain to produce earthquakes and displacements like those recorded in the trenches. Granted the given calculations are coupled with significant uncertainty, the consistency of the result along the arc is persuasive and consistent with prior recognition that geodetic slip now stored along much of the arc is sufficient to produce great earthquakes (e.g., Bilham *et al.*, 2001).

It has been suggested that scarps along the western portion of the arc may correspond to a historical earthquake that occurred in 1505 or 1344 (Jayangondaperumal *et al.*, 2017). Attributing the scarps to 1505, while intriguing, is not conclusive because historical records and isoseismal data are scant, limited primarily to damage reports in Tibetan villages north of the High Himalaya and reports of ground shaking in Agra (Jackson, 2002; Ambraseys and Jackson, 2003). The correlation of the scarps to the 1344 earthquake in western India is based on a single historical account ~400 km to the east in Kathmandu (Pant, 2002), so it is questionable. It has been $> \sim 500$ yr since the last large displacement along much of the western length of the arc whether or not the correlations are correct.

Based on instrumental estimates of an epicenter near Mt. Everest, distribution of damage and shaking reports, fault-plane solutions of more recent earthquakes exhibiting low-angle thrusting, and assumption of a 220 km × 120 km rupture plane, the $M_w > 8$ 1934 Bihar–Nepal earthquake has been attributed to ~5 m of slip on the MHT (Chen and Molnar, 1977; Molnar and Deng, 1984). The rupture area, though not well defined, has more recently been placed between ~85.5° E and 87.0° E longitude and reasoned to be a lesser size of 150 ± 25 km by 85 ± 10 km in dimension (Hough and Bilham, 2008), implying that coseismic slip in 1934 may have exceeded ~5 m. The crustal strain released by the 1934 event might serve to delay the time of the next expected surface rupture earthquake along this relatively small section of the arc (Fig. 1g).

The M_w 8.7 1950 Assam earthquake is the largest instrumentally recorded earthquake along the arc (Fig. 1a). Isoseismal and aftershock locations place the event at the eastern limit of the arc (Tandon, 1954). Relocation of aftershocks, analysis of waveforms, and consideration of the tectonic environment have led to the now generally cited interpretation that displacement during the event produced ~16 m of thrust motion on the easternmost 250×80 km^2 section of the north-dipping MHT (Chen and Molnar, 1977). The same authors (Chen and Molnar, 1977) cited the possibility that rupture extended yet further east and south around the sharp bend at the eastern end of the arc, an idea again put forth in a more recent study (Coudurier-Curveur *et al.*, 2020). Whether or not fault scarps along this

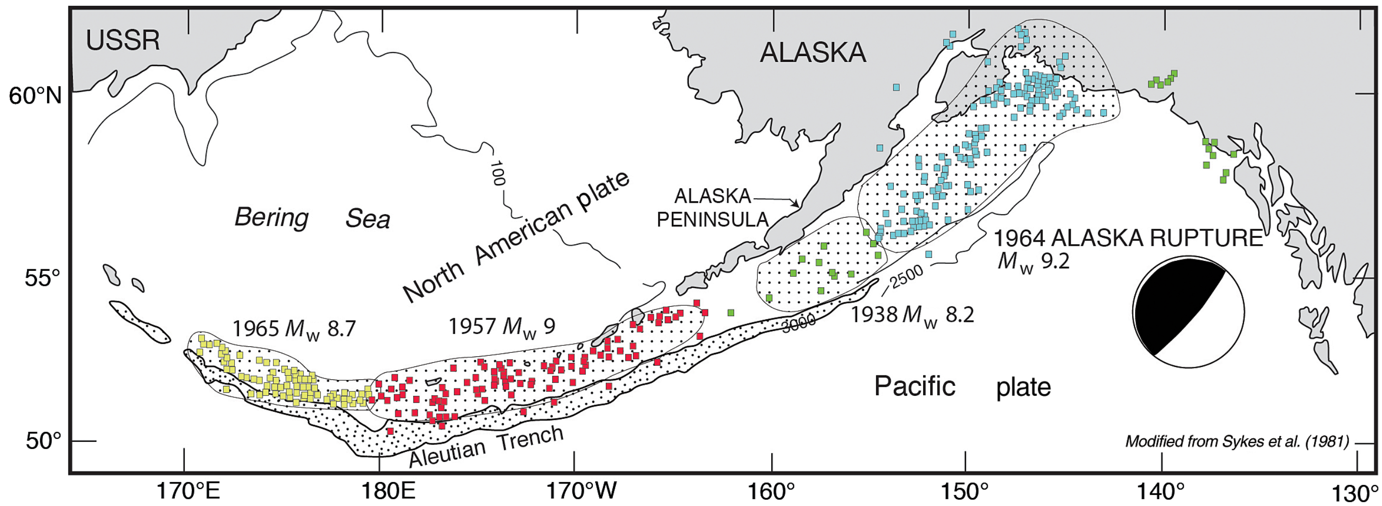

Figure 3. The sequence of great earthquakes (delineated by aftershock zones) that occurred during the twentieth century along the Aleutian subduction zone may serve as an analog for the expected occurrence of future great earthquakes along the Himalayan arc. The color version of this figure is available only in the electronic edition.

section of the HFT are the result of 1950 displacement remains to be decisively proven. Irrespective, the magnitude and associated coseismic displacement estimated for the 1950 earthquake are on the same order as that recorded in the numerous trench studies reported along the 2000 km length of the arc to the west (Table 1 and Fig. 1c).

Conclusion

To summarize, recorded surface rupture displacements are commensurate with earthquakes of $M_w \sim 8.5$ and greater with rupture lengths of 500 km and are likely greater (Table 1, Fig. 1c,d). Temporal constraints are insufficient to assess the exact extent of these past ruptures but do point to large-earthquake displacements clustering around the years A.D. 1200–1400 along major sections of the arc (Fig. 1f), a period of time notably shorter than the average repeat time of large surface rupture earthquakes along the arc. Estimates of the average repeat time between these displacements at any given site are generally in the range of 500–1000 yr (Fig. 1e), and the times when slip will accrue to the amount observed in the last great earthquakes along the arc are near today. The large size of past earthquakes and apparent occurrence in a time period shorter than the average time between repeated earthquakes lead to the suggestion that the arc is poised to rupture in a sequence of great earthquakes similar to that which occurred along the Aleutian Arc in the twentieth century (Sykes *et al.*, 1981) (Fig. 3). The M_w 8.7 1950 Assam earthquake might be considered the beginning of the sequence. Another such earthquake in the near future should not be a surprise, and the attendant human catastrophe stands to be unprecedented (Wyss *et al.*, 2018). Regrettably the temporal uncertainties in assessments like this remain on the order of human lifetimes.

Data and Resources

All data used in this article came from published sources listed in the references. The supplemental material for this article includes notes of clarification for Table 1 and a figure summarizing the paleoearthquake data used in constructing Figure 1.

Acknowledgments

This research was supported in part by National Science Foundation (NSF) Grant EAR-1345036. The synthesis arose with the kind invitation of Takashi Nakata to provide an overview of Himalayan paleoseismology at the Hokudan 2020 International Symposium on Active Faulting on the 25th anniversary of the Kobe earthquake. Roger Bilham and Roland Burgmann provided most constructive reviews and perspectives. Center for Neotectonics Contribution Number 79.

References

Almeida, R. V., J. Hubbard, L. Liberty, A. Foster, and S. N. Sapkota (2018). Seismic imaging of the Main Frontal Thrust in Nepal reveals a shallow decollement and blind thrusting, *Earth Planet. Sci. Lett.* **494,** 216–225.

Ambraseys, N., and D. Jackson (2003). A note on early earthquakes in northern India and southern Tibet, *Current Sci.* **84,** 570–582.

Arora, S., J. N. Malik, and S. Sahoo (2019). Paleoseismic evidence of a major earthquake event(s) along the hinterland faults: Pinjore Garden Fault (PGF) and Jhajra Fault (JF) in northwest Himalaya, India, *Tectonophysics* **757,** 108–122.

Berthet, T., G. Hetenyi, R. Cattin, S. N. Sapkota, C. Champollion, T. Kandel, E. Doerflinger, D. Drukpa, S. Lechmann, and M. Bonnin (2013). Lateral uniformity of India Plate strength over central and eastern Nepal, *Geophys. J. Int.* **195,** 1481–1493.

Bilham, R. (2019). Himalayan earthquakes: A review of historical seismicity and early 21st century slip potential, in *Himalayan*

Tectonics: A Modern Synthesis, P. J. Treloar and M. P. Searle (Editors), Geological Soc Publishing House, Bath, England, 423.

Bilham, R., V. K. Gaur, and P. Molnar (2001). Earthquakes – Himalayan seismic hazard, *Science* **293,** 1442–1444.

Bilham, R., K. M. Larson, and J. Freymueller (1997). GPS measurements of present day convergence across the Nepal Himalaya, *Nature* **386,** 61–64.

Blong, R., and R. Gillespie (1978). Fluvially transported charcoal gives erroneous ^{14}C ages for recent deposits, *Nature* **271,** 739–741.

Bollinger, L., S. N. Sapkota, P. Tapponnier, Y. Klinger, M. Rizza, J. Van der Woerd, D. R. Tiwari, R. Pandey, A. Bitri, and S. B. de Berc (2014). Estimating the return times of great Himalayan earthquakes in eastern Nepal: Evidence from the Patu and Bardibas strands of the Main Frontal Thrust, *J. Geophys. Res.* **119,** 7123–7163.

Chen, W.-P., and P. Molnar (1977). Seismic moments of major earthquakes and the average rate of slip in central Asia, *J. Geophys. Res.* **82,** 2945–2969.

Coudurier-Curveur, A., P. Tapponnier, E. Okal, J. Van der Woerd, E. Kali, S. Choudhury, S. Baruah, M. Etchebes, and C. Karakas (2020). A composite rupture model for the great 1950 Assam earthquake across the cusp of the East Himalayan Syntaxis, *Earth Planet. Sci. Lett.* **531,** 12.

Hossler, T., L. Bollinger, S. N. Sapkota, J. Lave, H. K. Gupta, and T. P. Kandel (2016). Surface ruptures of large Himalayan earthquakes in western Nepal: Evidence along a reactivated strand of the Main Boundary Thrust, *Earth Planet. Sci. Lett.* **434,** 187–196.

Hough, S. E., and R. Bilham (2008). Site response of the Ganges basin inferred from re-evaluated macroseismic, observations from the 1897 Shillong, 1905 Kangra, and 1934 Nepal earthquakes, *J. Earth Syst. Sci.* **117,** 773–782.

Ingleby, T., T. J. Wright, A. Hooper, T. J. Craig, and J. R. Elliott (2020). Constraints on the geometry and frictional properties of the Main Himalayan Thrust using coseismic, postseismic, and interseismic deformation in Nepalic deformation in Nepal, *J. Geophys. Res.* **125,** e2019JB019201, doi: 10.1029/2019JB019201.

Isacks, B., J. Oliver, and L. R. Sykes (1968). Seismology and new global tectonics, *J. Geophys. Res.* **73,** 5855–5899.

Iyengar, R. N., D. Sharma, and J. M. Siddiqui (1999). Earthquake History of India in medieval times, *Indian J. Hist. Sci.* **34,** 181–237.

Jackson, D. (2002). The great western-Himalayan earthquake of 1505: A rupture of the central Himalayan Gap?, in Tibet, past and present: Tibetan studies 1, *Proc. of the Ninth Seminar of the International Association for Tibetan Studies*, Leiden, Netherlands, 147–158.

Jayangondaperumal, R., R. L. Daniels, and T. M. Niemi (2017). A paleoseismic age model for large-magnitude earthquakes on fault segments of the Himalayan Frontal Thrust in the Central Seismic Gap of northern India, *Quarter. Int.* **462,** 130–137.

Jayangondaperumal, R., S. G. Wesnousky, and B. K. Choudhuri (2011). Near-surface expression of early to late Holocene displacement along the northeastern Himalayan Frontal thrust at Marbang Korong Creek, Arunachal Pradesh, India, *Bull. Seismol. Soc. Am.* **101,** 3060–3064.

Kumahara, Y., and R. Jayangondaperumal (2013). Paleoseismic evidence of a surface rupture along the northwestern Himalayan Frontal Thrust (HFT), *Geomorphology* **180,** 47–56.

Kumar, S., S. G. Wesnousky, R. Jayangondaperumal, T. Nakata, Y. Kumahara, and V. Singh (2010). Paleoseismological evidence of surface faulting along the northeastern Himalayan front, India: Timing, size, and spatial extent of great earthquakes, *J. Geophys. Res.* **115,** 20.

Kumar, S., S. G. Wesnousky, T. K. Rockwell, R. W. Briggs, V. C. Thakur, and R. Jayangondaperumal (2006). Paleoseismic evidence of great surface rupture earthquakes along the Indian Himalaya, *J. Geophys. Res.* **111,** no. B03304, doi: 10.1029/2004JB003309.

Kumar, S., S. G. Wesnousky, T. K. Rockwell, D. Ragona, V. C. Thakur, and G. G. Seitz (2001). Earthquake Recurrence and Rupture Dynamics of Himalayan Frontal Thrust, India, *Science* **294,** 2328–2331.

Lave, J., D. Yule, S. N. Sapkota, K. Basant, C. Madden, M. Attal, and R. Pandey (2005). Evidence for a Great Medieval Earthquake (~1100 A.D.) in the Central Himalayas, Nepal, *Science* **307,** 1302–1305.

Leonard, M. (2010). Earthquake fault scaling: Self-consistent relating of rupture length, width, average displacement, and moment release, *Bull. Seismol. Soc. Am.* **100,** 1971–1988.

Lindsey, E. O., R. Almeida, R. Mallick, J. Hubbard, K. Bradley, L. L. Tsang, Y. Liu, R. Burgmann, and E. M. Hill (2018). Structural control on downdip locking extent of the Himalayan megathrust, *J. Geophys. Res.* **123,** 5265–5278.

Lyon-Caen, H., and P. Molnar (1985). Gravity-anomalies, flexure of the Indian plate, and the structure, support and evolution of the Himalaya and Ganga basin, *Tectonics* **4,** 513–538.

Malik, J. N., T. Nakata, G. Philip, N. Suresh, and N. S. Virdi (2008). Active fault and paleoseismic investigation: Evidence of a historic earthquake along Chandigarh fault in the Frontal Himalayan zone, NW India, *Himalayan Geol.* **29,** 109–117.

Malik, J. N., A. K. Sahoo, A. A. Shah, D. P. Shinde, N. Juyal, and A. K. Singhvi (2010). Paleoseismic evidence from trench investigation along Hajipur fault, Himalayan Frontal Thrust, NW Himalaya: Implications of the faulting pattern on landscape evolution and seismic hazard, *J. Struct. Geol.* **32,** 350–361.

Malik, J. N., A. A. Shah, A. K. Sahoo, B. Puhan, C. Banerjee, D. P. Shinde, N. Juyal, A. K. Singhvi, and S. K. Rath (2010). Active fault, fault growth and segment linkage along the Janauri anticline (frontal foreland fold), NW Himalaya, India, *Tectonophysics* **483,** 327–343.

Molnar, P., W.-P. Chen, T. J. Fitch, P. Tapponnier, W. E. K. Warsi, and F. T. Wu (1977). Structure and tectonics of the Himalaya: A brief summary of geophysical observations, Colloques Internationaux du D.N.R.S., *Ecol. Geol. Himalaya* **268,** 269–294.

Molnar, P., and Q. D. Deng (1984). Faulting associated with large earthquakes and the average rate of deformation in central and eastern Asia, *J. Geophys. Res.* **89,** 6203–6227.

Molnar, P., and H. Lyon-Caen (1983). Constraints on the structure of the Himalaya from an analysis of gravity anomalies and a flexural model of the lithosphere, *J. Geophys. Res.* **88,** 8171–8191.

Mugnier, J. L., P. Huyghe, A. P. Gajurel, and D. Becel (2005). Frontal and piggy-back seismic ruptures in the external thrust belt of Western Nepal, *J. Asian Earth Sci.* **25,** 707–717.

Nakata, T. (1972). *Geomorphic history and crustal movements of the foot-hills of the Himalayas*, *Sci. Rep.*, Tohoku Univ., 7th Ser, 22, 39-177.

Nakata, T. (1989). *Active Faults of the Himalaya of India and Nepal, Geological Society of America Special Paper*, Vol. 232, 243–264.

Pant, M. R. (2002). *A Step towards a Historical Seismicity of Nepal, in ADARSA*, Pundit Publications, Kathmandu, 29–60.

Powers, P. M., R. J. Lillie, and R. S. Yeats (1998). Structure and shortening of the Kangra and Dehra Dun reentrants, sub-Himalaya, India, *Geol. Soc. Am. Bull.* **110,** 1010–1027.

Priyanka, R. S., R. Jayangondaperumal, A. Pandey, R. L. Mishra, I. Singh, R. Bhushan, P. Srivastava, S. Ramachandran, C. Shah, S. Kedia, *et al.* (2017). Primary surface rupture of the 1950 Tibet-Assam great earthquake along the eastern Himalayan front, India, *Sci. Rep.* **7,** 12.

Raiverman, V., A. K. Srivastava, and D. N. Prasad (1993). On the foothill thrust of northwestern Himalaya, *J. Himalayan Geol.* **4,** 237–256.

Rajendran, C. P., B. John, and K. Rajendran (2015). Medieval pulse of great earthquakes in the central Himalaya: Viewing past activities on the frontal thrust, *J. Geophys. Res.* **120,** 1623–1641.

Rajendran, K., R. M. Parameswaran, and C. P. Rajendran (2017). Seismotectonic perspectives on the Himalayan arc and contiguous areas: Inferences from past and recent earthquakes, *Earth-Sci. Rev.* **173,** 1–30.

Ramsey, C. (1995). Radiocarbon calibration and analysis of stratigraphy: The OxCal program, *Radiocarbon* **37,** 425–430.

Ramsey, C. (2009). Bayesian analysis of radiocarbon dates, *Radiocarbon* **51,** 337–360.

Rao, Y. S., A. A. Rahman, and D. P. Rao (1974). On the structure of the Siwalik range between rivers Yamuna and Ganga, *Himalayan Geol.* **4,** 137–150.

Reimer, P. J., E. Bard, A. Bayliss, J. W. Beck, P. G. Blackwell, C. B. Ramsey, C. E. Buck, H. Cheng, R. L. Edwards, M. Friedrich, *et al.* (2013). INTCAL13 and marine13 radiocarbon age calibration curves 0-50,000 years Cal Bp, *Radiocarbon* **55,** 1869–1887.

Seeber, L., and J. Armbruster (1981). Great detachment earthquakes along the Himalayan arc and long-term forecasting, in *Earthquake Prediction: An International Review*, D. W. Simpson and P. G. Richards (Editors), AGU, Washington, D. C., 215–242.

Sykes, L. R., J. B. Kisslinger, L. S. House, J. N. Davies, and K. H. Jacob (1981). Rupture zones and repeat times of great earthquakes along the Alaska-Aleutian Arc, 1784-1980, in *Earthquake Prediction: An international Review*, D. W. Simpson and P. G. Richards (Editors), American Geophysical Union, Washington D. C., 73–80.

Tandon, A. N. (1954). The study of the great Assam earthquake of August, 1950, *Ind. J. Met. Geophys.* **5,** 95–137.

Upreti, B. N., T. Nakata, Y. Kumahara, H. Yagi, K. Okumura, T. K. Rockwell, and N. S. Virdi (2000). The latest active faulting in Southeast Nepal, *Proc. of the Hokudan International Symposium and School in Active Faulting*, Awaji Island, Hyogo Japan, 533–536.

Vernant, P., R. Bilham, W. Szeliga, D. Drupka, S. Kalita, A. K. Bhattacharyya, V. K. Gaur, P. Pelgay, R. Cattin, and T. Berthet (2014). Clockwise rotation of the Brahmaputra Valley relative to India: Tectonic convergence in the eastern Himalaya, Naga Hills, and Shillong Plateau, *J. Geophys. Res.* **119,** 6558–6571.

Wesnousky, S. G. (2008). Displacement and geometrical characteristics of earthquake surface ruptures: Issues and implications for seismic-hazard analysis and the process of earthquake rupture, *Bull. Seismol. Soc. Am.* **98,** 1609–1632.

Wesnousky, S. G., Y. Kumahara, D. Chamlagain, and P. C. Neupane (2019). Large Himalayan Frontal Thrust paleoearthquake at Khayarmara in eastern Nepal, *J. Asian Earth Sci.* **174,** 346–351.

Wesnousky, S. G., Y. Kumahara, D. Chamlagain, I. K. Pierce, A. Karki, and D. Gautam (2017a). Geological observations on large earthquakes along the Himalayan frontal fault near Kathmandu, Nepal, *Earth Planet. Sci. Lett.* **457,** 366–375.

Wesnousky, S. G., Y. Kumahara, D. Chamlagain, I. K. Pierce, T. Reedy, S. J. Angster, and B. Giri (2017b). Large paleoearthquake timing and displacement near Damak in eastern Nepal on the Himalayan Frontal Thrust, *Geophys. Res. Lett.* **44,** 8219–8226.

Wesnousky, S. G., S. Kumar, R. Mohindra, and V. C. Thakur (1999). Uplift and convergence along the Himalayan frontal thrust of India, *Tectonics* **18,** 967–976.

Wesnousky, S. G., S. Kumahara, T. Nakata,, D. Chamlagain,, and P. Neupane (2018). New observations disagree with previous interpretations of surface rupture along the Himalayan Frontal Thrust during the great 1934 Bihar-Nepal earthquake,, *Geophys. Res. Lett.*. **45,** 2652–2658.

Wyss, M., S. Gupta, and P. Rosset (2018). Casualty estimates in repeat Himalayan earthquakes in India, *Bull. Seismol. Soc. Am.* **108,** 2877–2893.

Yule, D., S. Dawson, J. Lave, S. N. Sapkota, and D. R. Tiwari (2006). Possible evidence for surface rupture of the Main Frontal Thrust during the great 1505 Himalayan earthquake, far-western Nepal, *EOS Trans. AGU, Fall Meeting 2006*, San Francisco, California, December 2006, Abstract S33C-05.

Zheng, G., H. Wang, T. J. Wright, Y. D. Lou, R. Zhang, W. X. Zhang, C. Shi, J. F. Huang, and N. Wei (2017). Crustal deformation in the India-Eurasia Collision Zone from 25 years of GPS measurements, *J. Geophys. Res.* **122,** 9290–9312.

Manuscript received 26 May 2020
Published online 19 August 2020